IOP Conference Series: Materials Science and Engineering

Depolymerisation of liquid epoxidized natural rubber (LENR) using lanthanum hydroxide ($La(OH)_3$)-HNT Catalyst

IOP Conf. Series: Materials Science and Engineering **509** (2019) 012104 doi:10.1088/1757-899X/509/1/012104

Depolymerisation of liquid epoxidized natural rubber (LENR) using lanthanum hydroxide ($La(OH)_3$)-HNT Catalyst

Nur Najwa Abdul Talib[1], Noor Hana Hanif Abu Bakar[1], Mohamad Abu Bakar[1], A. Iqbal[1], N.H Yusof[2]

[1] Faculty of Chemical Science, Universiti Sains Malaysia, Universiti Sains Malaysia, Penang 11800, Malaysia
[2] Malaysian Rubber Board, Sungai Buluh, 47000 Sungai Buluh, Malaysia
* Corresponding author: hana_hanif@usm.my

Abstract. A simple and versatile method is reported for the synthesis of $La(OH)_3$ on halloysite nanotubes (HNT) for the catalytic depolymerization of liquid epoxidized natural rubber (LENR). The lanthanum nitrate was incorporated into HNT by impregnation method. The characteristics of these $La(OH)_3$–HNT catalysts were investigated by using SEM equipped with Energy Dispersive X-ray (EDX), X-Ray Fluorescence (XRF), Fourier-transform Infrared Spectroscopy (FTIR), X-Ray Diffraction (XRD), Ultraviolet Visible Light (UV-Vis) and Photoluminescence (PL). The obtained results confirm the presence of $La(OH)_3$ on the surface of HNT. The presence of $La(OH)_3$ -HNT in the LENR exhibited excellent depolymerization reaction resulting in a reduction of the average molecular weight (M_w) from 18984 to 2111. The M_w was measured by gel permeation chromatography (GPC).
Keywords: Depolymerization, LENR, Lanthanum hydroxide, $La(OH)_3$, HNT, catalyst

1. Introduction

Natural rubber (NR) is a biopolymer which consists of repeating monomer units of cis-1,4-isoprene that are randomly distributed along the polymer chain [1]. Having epoxy groups in the structure of NR results in a derivative which is known as epoxidized natural rubber (ENR) [2]. ENR consists of shorter polymeric chains compared to NR with part of the C=C being converted into epoxy group. Liquid epoxidized natural rubber (LENR) could be obtained from the degradation of ENR. Previously reported research on depolymerization of ENR requires a lower molar mass for effective use [3]. Since LENR is a liquid form of ENR with smaller molecular weight, LENR is the best solution used for depolymerization studies [4]. Scheme 1(a) illustrates the structure of NR and its derivative, LENR.

Various techniques have been used to study the degradation of polymer such as chemical degradation [5], pyrolysis [6], metathetic [7], co-gasification [8] and hydrogenation [5].The limitations of these processes are related to high usage of solvents, high temperature and pressure and various side reactions. Limited studies are available regarding catalytic degradation studies. Previously, studies have focused on the catalytic degradation of lignin in the presence of cerium, Ce and lanthanum, La on carbon nanotubes (CNT) as a catalyst [9]. The presence of catalyst helps the polymer chain to break effectively via the C-C bond. Similar investigations on the use of metal supported catalyst for polymer degradation such as waste tire [10], used palm oil [11], heavy oil [12], soybean oil [13], biomass tar [14] and guaiacol [15] are also available. A wide range of catalysts such as nickel, Ni [15], gold, Au [16], platinum, Pt [17], palladium, Pd [18], and ruthenium, Ru [19] can be employed to promote the catalytic degradation of polymers. The catalytic activity depends on several factors which include the type of metal employed

and the properties of the support used. HNT are natural occurring eco-friendly nanotubes that are formed over millions of years. The chemical structure of HNT is illustrated in scheme 1(b). Metal supported HNT has gained increasing attention lately due to its low cost [20]. Hence, in this study the performance of La species supported on HNT for the depolymerization of LENR is examined and the obtained degradation compound was investigated.

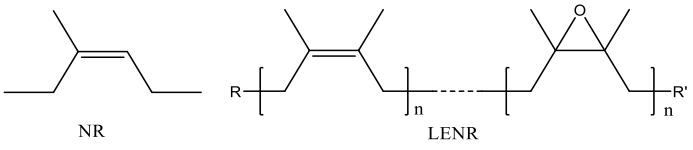

n = number of repeat units
R and R' are terminal groups

(a)

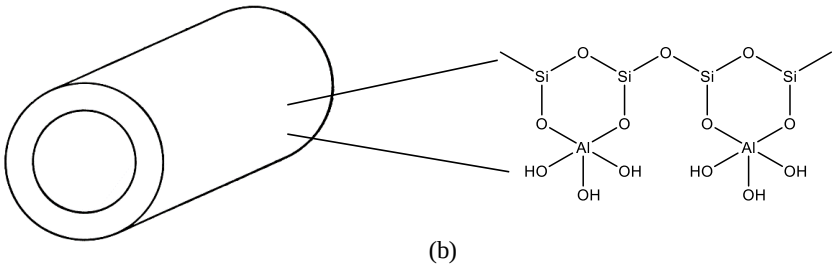

(b)

Scheme 1. Chemical structure of (a) LENR [21] and (b) HNT [22, 23].

2. Experimental

2.1. Materials

LENR with 50% of epoxidation was obtained as a gift from Malaysian Rubber Board. HNT with 99% purity was purchased from Sigma Aldrich, US. Meanwhile, other chemicals such as toluene, chloroform and tetrahydrofuran (THF) used in this study were all obtained from QRëC^{TM}, Malaysia. The lanthanum nitrate hexahydrate salt, $La(NO_3)_3.6H_2O$ was purchased from Sigma Aldrich, US.

2.2. Preparation of catalyst

$La(NO_3)_3.6H_2O$ was used as starting material and HNT as a support. For the preparation of 0.5 M $La(NO_3)_3.6H_2O$ solution, 0.015 mol $La(NO_3)_3.6H_2O$ was weighed and dissolved in 10 mL distilled water. Then, 5 g HNT was impregnated in 7.18 mL of 0.5 M $La(NO_3)_3.6H_2O$ solution for the preparation of La^{3+}-HNT and stirred for 24 h. The mixture was then dried in air overnight and then dried in an oven at 50°C for 3 days for the formation of $La(OH)_3$-HNT. After grinding, the catalyst was stored in a desiccator before use. XRF analysis revealed the La content as 9.24 wt%. Hence the catalyst was denoted as 9.25 wt% $La(OH)_3$-HNT.

2.3. Depolymerization of LENR

About 1 g of LENR was dissolved in 20 ml of toluene. The solution was transferred into a 30 mL Teflon-lined reactor and mixed with 0.5 g of $La(OH)_3$-HNT catalyst. The mixture was heated for 2 to 6 hours at different temperatures between 150 and 250℃ in a furnace. After that, the mixture was cooled to room temperature and then was centrifuged for 5 to 10 minutes at 3500 rpm. The product was vacuum dried for 3 days at room temperature. The products were analysed with GPC.

2.4. Characterization

The chemical compositions of the prepared catalysts were obtained by X-ray fluorescence spectroscopy (XRF) analysis to determine the percentage of La metal on the HNT. A PanAlytical Axios Mas

(Holland) XRF equipped with a rhodium tube and beryllium window was employed. The XRD analysis was conducted on a Bruker D8 Advance X-ray powder diffractometer with a Cu–Kα radiation (λ=1.54 Å, 40 kV, 40 mA) in the 2θ range of 10°-90°. A *Perkin Elmer* Fourier Transform Infrared (FTIR) with attenuated total reflectance (ATR) technique was used for the analysis of the functional group presence. The spectra were measured at the range from 600 to 4000 cm^{-1} at room temperature. The UV-Vis diffuse reflection spectra were obtained for a dry-pressed disk sample using a Perkin Elmer Lambda 35. Fluorescence measurements were performed using a Perkin Elmer LS55 Fluorescence spectrometer. The surface morphology of the catalyst was observed by using a Quanta 650 scanning electron microscopy (SEM) (Holland) coupled with Energy Dispersive Spectroscopy (EDS) for further elements identification of the catalysts. The samples were sputter coated with gold using *Polaran (Fiscons) SC515, VG Microtech Susses Sputter Coated (United Kingdom).* The thermal decomposition of the $La(OH)_3$-HNT using a TGA/SDTA *851 Mettler Toledo* instrument in nitrogen atmosphere from 30 to 920°C at a heating rate of 20°C min^{-1}.*Agilent 1260 Infinity MDS GPC* was used to determine the average molecular weight (M_w) and average molecular number (M_n) of LENR using tetrahydrofuran (THF) as solvent at a flow rate of 1 ml min^{-1}.

3. Result and Discussion

3.1. X-Ray Diffraction (XRD)

The HNT as well as the catalyst prepared were inspected by using X-ray diffraction. Figure 1 shows the XRD trace in the 2θ range of 10°-90° for HNT and La species supported on HNT. The reflections in Figure 1(a) at 11.8°, 20.0°, 24.2°, 26.4°, 34.8°, 38.2°, 38.4°,54.5° and 62.5° are attributed to HNT [24]. As can be seen, the high intensity peak at 2θ of 11.8° corresponds to the d_{001} plane of HNT with a spacing of 7 Å [25].At this basal reflection, HNT is featuring a highly disordered tubular morphology, small crystal size and interstratifications of layer with different hydration states [26]. Other additional peaks are observed at the2θ value of 20°, 24.7° and 26.6°. The first two peaks are attributed to the d_{020} and d_{002} diffraction planes. However, all the peaks are attributed to a dehydrated HNT structure [27-29]. Other work reveal that the peak at 26.6° may also be due to quartz (SiO_2) available in a small amount, in the HNT [24].The presence of a peak at 62.5° indicates the dioctahedral mineral type of HNT [30]. Comparison of the XRD pattern of HNT with the catalyst shows no significant difference in terms of peak positions. Also, no diffraction peaks corresponding to any La species were observed. Previous studies reported that introducing La affected the crystal structure of the support by decreasing the intensity of the XRD peaks [31]. When La species was incorporated within HNT's tubular, the water molecules expel from the interlayer [28]. It is possible that in this case the intensity of the HNT peaks in the catalyst decreases as observed in Figure 1 (b).

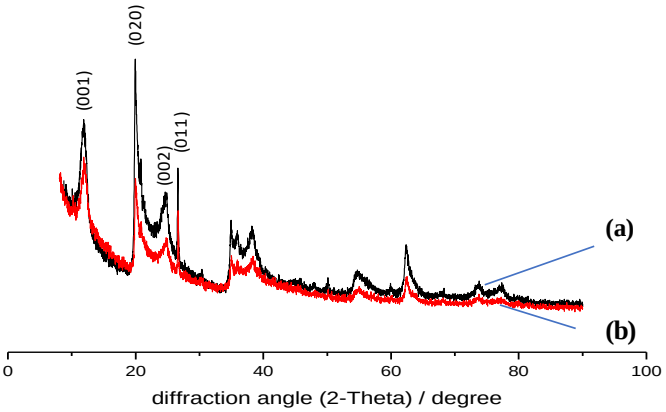

Figure 1. XRD diffraction patterns of (a) pristine HNT and (b) La catalyst.

3.2. Fourier-Transform Infrared Spectroscopy (FTIR)

To further confirm the La species in the catalyst, FTIR analysis was conducted. FTIR is an additional characterization technique which can aid in the confirmation of $La(OH)_3$.FTIR spectrum of HNT and $La(OH)_3$-HNT is depicted in Figure 2. As can be seen in Figure 2(a), HNT has peaks at 678, 750, 792, 904, 999, 1118, 1648, 3550, 3623 and 3691 cm^{-1}. The strong absorption at 999 cm^{-1}due to the O-Si-O siloxane surface group. The peaks at 3623 and 3691 cm^{-1} are attributed to Al-OH stretching bands and 1118 cm^{-1} is due to Si-O vibration, which are characteristic of HNTs. While the small shoulder at 3550 cm^{-1} could be related to OH groups H-bonded to interlayer water [32]. Other characteristic absorption peaks of pristine HNT, such as at 1646 correspond to O-H deformation of water, 904 cm^{-1} attributed to O-H deformation of hydroxyl groups, 792 cm^{-1} correspond to symmetric stretching of Si-O and 678 cm^{-1} correspond to perpendicular Si-O stretching are also seen [33, 34]. Comparison of the spectra in Figure 2(a) to the spectra of $La(OH)_3$-HNT in Figure 2(b) shows that similar peaks as HNT are observed. In addition, additional peaks are seen positioned at 1329, 1448, and 3424 cm^{-1}. The broad peak at 3424 cm^{-1} and the slightly broad peak at 1648 cm^{-1} are due to the O-H vibration from the absorbed water which occurs mostly on the surface of the active phase of the catalyst. Previous studies of $La(OH)_3$ shows similar trends [35]. Also, the 1329 cm^{-1} peak has been attributed to the bending mode of O-H [35]. However other works have reported that this absorption peak is assigned to the vibration of NO^{3-} anions which exist due to the La^{3+} salt [36]. In contrast, the peak at about 1448 cm^{-1} can be attributed to the carbonate groups which form from the reaction of $La(OH)_3$ with CO_2 from air during the analysis procedure [36]. $La(OH)_3$ also exhibit peaks at 3613, 1635 and660 cm^{-1} due to the stretching and bending O-H vibration of $La(OH)_3$, O-H vibration from the absorbed water on the surface and bending vibration of La-O-H. However, these peaks coincide with the peaks of HNT. Based on the FTIR, it is possible that $La(OH)_3$ exists, however further confirmation is required.

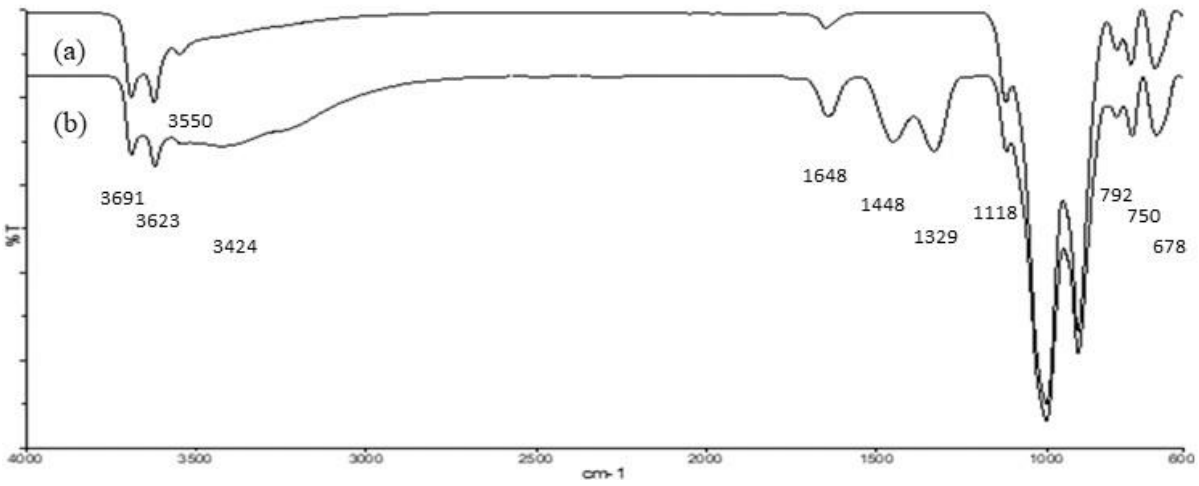

Figure 2. FTIR spectrum for 9.25 wt% of (a) pristine HNT and (b) $La(OH)_3$-HNT catalyst.

3.3. Ultraviolet Visible Light (UV-Vis) and Photoluminescence (PL) Spectroscopy

The UV-Vis and PL properties of $La(OH)_3$-HNT was investigated to observe the formation of $La(OH)_3$-HNT.The optical absorbance and PL measurement were carried out, as shown in Figure 3. As can be seen in Figure 3(a) HNT has an absorbance peak at 250 nm while $La(OH)_3$-HNT shows that the absorption spectrum appears at 224 nm. Previous work reported that the absorbance band for $La(OH)_3$ is present at 237 nm [37]. Hence this work shows that the peak for the catalyst is slightly shifted. This might be due to the presence of HNT with $La(OH)_3$. To further confirm the presence of $La(OH)_3$ on HNT, PL measurement was carried out at room temperature. As shown in Figure 3(b), at 230 nm excitation wavelength, HNT show strong PL emission at 460 nm and small PL emission at 689 nm. However, at an excitation wavelength of 230 nm, $La(OH)_3$-HNTshows a strong PL emission peak at

460 nm and smaller peaks at 692 nm, 414 nm, 371 nm and 314 nm. Emission peaks at 460 and 692 nm can be attributed to HNT. However, the peak at 692 may also attributed to $La(OH)_3$. A previous work has shown that $La(OH)_3$ exhibits a strong emission peak at 715 nm when excited at a wavelength of 237 nm [37]. In this sample, other smaller peaks at 414 nm, 371 nm and 314 also appeared. Similar PL emission due to the presence of $La(OH)_3$ in the sample was reported [37, 38].

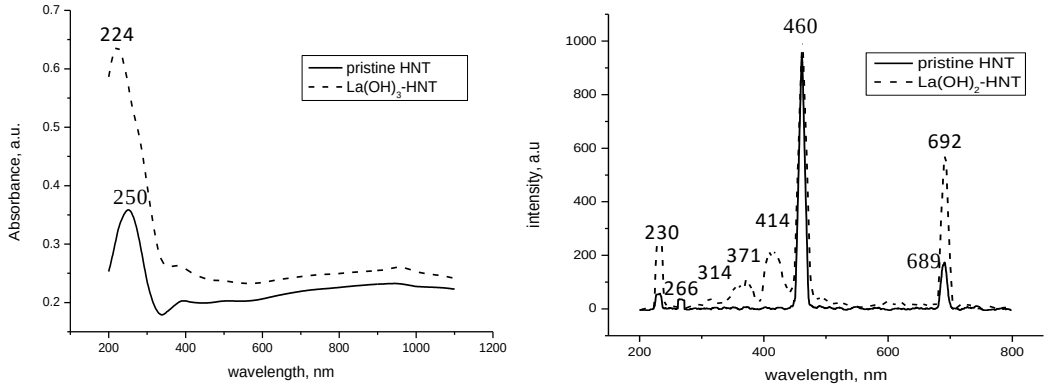

Figure 3. (a) UV-Vis absorption spectrum of $La(OH)_3$ and (b) PL emission spectrum of $La(OH)_3$ with 1% attenuator.

3.4. SEM-EDX analysis

SEM and EDX analysis was conducted to ensure the presence of $La(OH)_3$. This is exhibited in Figure 4. EDX results reveal that silicon, Si, aluminium, Al, oxygen, O and La elements are available. The presence of Al, silicon, Si and O are attributed to the HNT while O can be attributed to both HNT and $La(OH)_3$.

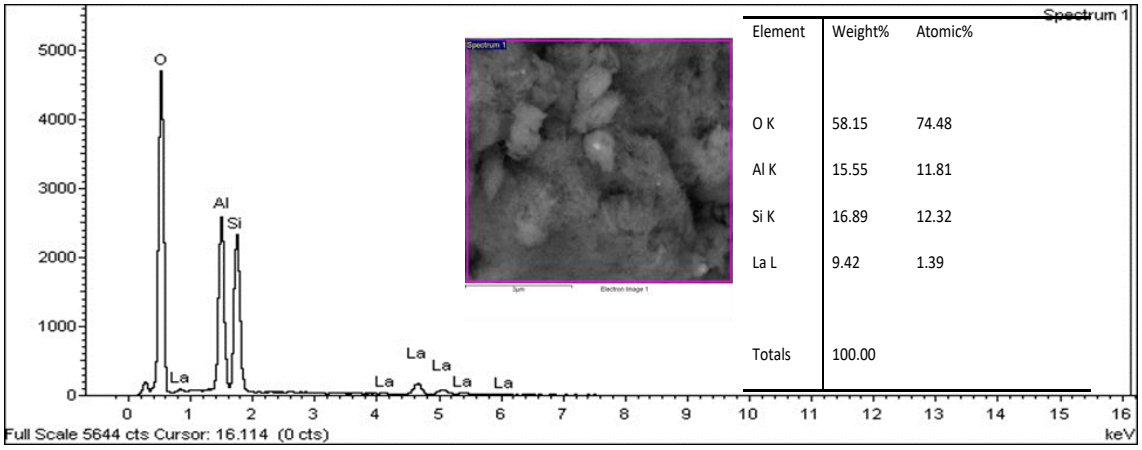

Figure 4. EDX result of $La(OH)_3$ -HNT catalyst.

3.5. Thermal Gravimetric Analysis

Thermal gravimetric analysis (TGA) was conducted to further study the thermal stability of HNTs and $La(OH)_3$-HNTs. The T_{max} values are tabulated in Table 1. A two-step weight loss stage can be identified in the HNT sample. Between the range of 30 and 100°C, the weight loss can be related to the loss of water from the HNT surface [27]. The major weight loss over the range of 400 to 600°C for HNT is attributed to the dihydroxylation of Al-OH group of halloysite [39]. Subsequently, the 9.25 wt% $La(OH)_3$-HNT shows several weight loss stages occurs at four maximum temperatures which are 58, 311, 383 and 490°C. The first interval coheres to elimination of physically adsorbed water at below temperature 150°C [36]. Secondly, the removal of structural water from $La(OH)_{(3-x)}(NO_3)_x$ occurs

between 200 and 380°C [36]. Between temperature 380 and 500°C, the weight loss is due to the removal of the residual structure water from $LaO(OH)_{(1-x)}(NO_3)_x$ [36]. Lastly, final weight loss at 490°C corresponds to HNT. It can be said that the first and last weight loss coincides with the peaks of HNT. Above 500°C, the weight loss can also be related to the removal of nitrate from the structure [36].

Table 1. Temperature maximum for HNT and $La(OH)_3$-HNT.

Sample	$T_{onset\ 1}$(°C)	$T_{max\ 1}$(°C)	$T_{onset\ 2}$ (°C)	$T_{max\ 22}$(°C)	$T_{onset\ 3}$(°C)	$T_{max\ 3}$(°C)	$T_{onset\ 4}$(°C)	$T_{max\ 4}$(°C)
HNT	47	49	481	493				
$La(OH)_3$-HNT	55	58	304	311	376	383	478	490

3.6. Catalytic studies - Gel Permeation Chromatography (GPC).

The sample was further inspected using GPC analysis to further study average molecular weight (M_n) and weight average molecular weight (M_w). The (M_n) and (Mw) of pristine LENR and its depolymerized derivative were determined. The data of M_n, M_w and polydispersity index, PDI are summarized in Table 2. PDI is the ratio of M_w to M_n. According to GPC value, the presence of $La(OH)_3$-HNT in the LENR at optimum condition of 200°C for 4 h of reaction exhibited excellent depolymerization reaction. The value of M_w of LENR reduced from 18984 to 2111. The polymer chain depolymerized due to the presence of $La(OH)_3$-HNT catalyst in the system.

Table 2. Change in molecular weight after degradation of LENR.

Sample	Mn	Mw	PDI (M_w/M_n)
LENR	9150	18984	2.07
LENR+$La(OH)_3$-HNT	691	2111	3.05

4. Conclusions

The 9.25 wt% of $La(OH)_3$ was successfully prepared through impregnation method. FTIR, and PL confirm the presence of $La(OH)_3$ on HNT. The thermal decomposition of $La(OH)_3$ was investigated by TG/DTG studies and these confirmed the four-step mechanism of $La(OH)_3$-HNT. $La(OH)_3$ underwent complete decomposition at about 500°C. Subsequently, the presence of $La(OH)_3$-HNT successfully depolymerized LENR. The M_w of LENR was reduced from 18984 to 2111. Hence the findings of the present work give good performance of $La(OH)_3$ supported on HNT in depolymerization of LENR. These results suggest the potential of $La(OH)_3$ work with other metal as bimetallic catalyst supported on HNT towards depolymerized of LENR.

Acknowledgements

The authors would like to acknowledge Universiti Sains Malaysia (USM) for the Bridging Grant (304.PKIMIA.6316051) and School of Chemical Sciences, USM for their facilities. Also, to Ministry of Higher Education through MyPhD Scholarship as a financial support.

References

[1] Hamzah R, Bakar M A, Khairuddean M, Mohammed I A and Adnan R 2012 A structural study of epoxidized natural rubber (ENR-50) and its cyclic dithiocarbonate derivative using NMR spectroscopy techniques *Molecules* **17** 9 10974-93

[2] Baker C and Gelling I 1987 *Developments in Rubber Technology—4,* ed A Whelan and K S Lee (Dordrecht: Springer) pp 87-117

[3] Fainleib A, Pires R V, Lucas E F and Soares B G 2013 Degradation of non-vulcanized natural rubber-renewable resource for fine chemicals used in polymer synthesis *Polímeros* **23** 4 441-50

[4] Azhar N H A, Rasid H M, Tahir N A M and Yusoff S F M 2017 Penghidrogenan in situ getah

asli cecair terepoksida menggunakan diimida *Malays. J. Anal. Sci.* **21** 6 1380-8
[5] Ahmad N, Abnisa F and Daud W M A W 2016 Potential use of natural rubber to produce liquid fuels using hydrous pyrolysis–a review *RSC Adv.* **6** 73 68906-21
[6] Basu P 2010 *Biomass gasification and pyrolysis: practical design and theory*: Academic press)
[7] Mouawia A, Nourry A, Gaumont A-C, Pilard J-F o and Dez I 2016 Controlled Metathetic Depolymerization of Natural Rubber in Ionic Liquids: From Waste Tires to Telechelic Polyisoprene Oligomers *ACS Sustain. Chem. Eng.* **5** 1 696-700
[8] Peres A P G, Lunelli B and Fllho R 2013 Application of biomass to hydrogen and syngas production *Chem. Eng. Trans.* **32** 589-94
[9] Ma Q, Liu Q, Li W, Ma L, Wang J, Liu M and Zhang Q 2017 Catalytic depolymerization of lignin for liquefied fuel at mild condition by rare earth metals loading on CNT *Fuel Process. Technol.* **161** 220-5
[10] Rowhani A and Rainey T 2016 Scrap tyre management pathways and their use as a fuel—a review *Energies* **9** 11 888
[11] Taufiqurrahmi N, Mohamed A R and Bhatia S 2010 Deactivation and coke combustion studies of nanocrystalline zeolite beta in catalytic cracking of used palm oil *Chem. Eng. J.* **163** 3 413-21
[12] Kondoh H, Tanaka K, Nakasaka Y, Tago T and Masuda T 2016 Catalytic cracking of heavy oil over TiO2–ZrO2 catalysts under superheated steam conditions *Fuel* **167** 288-94
[13] Emori E Y, Hirashima F H, Zandonai C H, Ortiz-Bravo C A, Fernandes-Machado N R C and Olsen-Scaliante M H N 2017 Catalytic cracking of soybean oil using ZSM5 zeolite *Catal. Today* **279** 168-76
[14] Liu H, Chen T, Chang D, Chen D, Kong D, Zou X and Frost R L 2012 Effect of preparation method of palygorskite-supported Fe and Ni catalysts on catalytic cracking of biomass tar *Chem. Eng. J.* **188** 108-12
[15] Fang H, Zheng J, Luo X, Du J, Roldan A, Leoni S and Yuan Y 2017 Product tunable behavior of carbon nanotubes-supported Ni–Fe catalysts for guaiacol hydrodeoxygenation *Appl. Catal. A Gen.* **529** 20-31
[16] Qi C, Wang Y, Ding X and Su H 2016 Catalytic cracking of light diesel over Au/ZSM-5 catalyst for increasing propylene production *Chin. J. Catal.* **37** 10 1747-54
[17] Zhang H, Wang Z, Li S, Jiao Y, Wang J, Zhu Q and Li X 2017 Correlation between structure, acidity and activity of Mo-promoted Pt/ZrO2-TiO2-Al2O3 catalysts for n-decane catalytic cracking *Appl. Therm. Eng.* **111** 811-8
[18] Bhogeswararao S and Srinivas D 2015 Catalytic conversion of furfural to industrial chemicals over supported Pt and Pd catalysts *J. Catal.* **327** 65-77
[19] Kim M, Son D, Choi J-W, Jae J, Suh D J, Ha J-M and Lee K-Y 2017 Production of phenolic hydrocarbons using catalytic depolymerization of empty fruit bunch (EFB)-derived organosolv lignin on Hβ-supported Ru *Chem. Eng. J.* **309** 187-96
[20] Yuan P, Tan D and Annabi-Bergaya F 2015 Properties and applications of halloysite nanotubes: recent research advances and future prospects *Appl. Clay Sci.* **112** 75-93
[21] Kargarzadeh H, Ahmad I, Abdullah I, Thomas R, Dufresne A, Thomas S and Hassan A 2015 Functionalized liquid natural rubber and liquid epoxidized natural rubber: A promising green toughening agent for polyester *J. Appl. Polym. Sci.* **132** 3
[22] Abdullayev E and Lvov Y 2010 Clay nanotubes for corrosion inhibitor encapsulation: release control with end stoppers *J. Mater. Chem.* **20** 32 6681-7
[23] Hebbar R S, Isloor A M, Ananda K and Ismail A 2016 Fabrication of polydopamine functionalized halloysite nanotube/polyetherimide membranes for heavy metal removal *J. Mater. Chem. A* **4** 3 764-74
[24] Wu X, Liu C, Qi H, Zhang X, Dai J, Zhang Q, Zhang L, Wu Y and Peng X 2016 Synthesis and adsorption properties of halloysite/carbon nanocomposites and halloysite-derived carbon nanotubes *Appl. Clay Sci.* **119** 284-93

[25] Alhuthali A and Low I M 2013 Influence of halloysite nanotubes on physical and mechanical properties of cellulose fibres reinforced vinyl ester composites *J. Reinf. Plast. Compos.* **32** 4 233-47
[26] Joussein E, Petit S, Churchman J, Theng B, Righi D and Delvaux B 2005 Halloysite clay minerals–a review *Clay Minerals* **40** 383-426
[27] Garcia-Garcia D, Ferri J M, Ripoll L, Hidalgo M, Lopez-Martinez J and Balart R 2017 Characterization of selectively etched halloysite nanotubes by acid treatment *Appl. Surf. Sci.* **422** 616-25
[28] Sun P, Liu G, Lv D, Dong X, Wu J and Wang D 2015 Effective activation of halloysite nanotubes by piranha solution for amine modification via silane coupling chemistry *RSC Adv.* **5** 65 52916-25
[29] Zango Z, Garba Z N, Bakar N A, Tan W and Bakar M A 2016 Adsorption studies of Cu2+–Hal nanocomposites for the removal of 2, 4, 6-trichlorophenol *Appl. Clay Sci.* **132** 68-78
[30] Ismail H, Pasbakhsh P, Ahmad Fauzi M and Abu Bakar A 2009 The effect of halloysite nanotubes as a novel nanofiller on curing behaviour, mechanical and microstructural properties of ethylene propylene diene monomer (EPDM) nanocomposites *Polym. Plast. Technol. Eng.* **48** 3 313-23
[31] Rahul R, Satyarthi J K and Srinivas D 2011 Lanthanum and zinc incorporated hydrotalcites as solid base catalysts for biodiesel and biolubricants production *Indian J. Chem. A* **50A** 1017-25
[32] Mondragón M, Cortes M A, Arias E, Falcony C and Zelaya-Angel O 2011 Photoluminescence of epoxy/clay nanocomposites *Polym. Eng. Sci.* **51** 9 1808-14
[33] Arat R and Uyanık N 2017 Surface modification of nanoclays with styrene-maleic anhydride copolymers *Nat. Resour.* **8** 03 159
[34] Tzounis L, Herlekar S, Tzounis A, Charisiou N D, Goula M and Stamm M 2017 Halloysite Nanotubes Noncovalently Functionalised with SDS Anionic Surfactant and PS-b-P4VP Block Copolymer for Their Effective Dispersion in Polystyrene as UV-Blocking Nanocomposite Films *J. Nanomater.* **2017**
[35] Hussain S K, Nagaraju G, Pavitra E, Raju G S R and Yu J S 2015 La (OH) 3: Eu 3+ and La 2 O 3: Eu 3+ nanorod bundles: growth mechanism and luminescence properties *CrystEngComm* **17** 48 9431-42
[36] Aghazadeh M, Golikand A N, Ghaemi M and Yousefi T 2011 La2O3 nanoplates prepared by heat-treatment of electrochemically grown La (OH) 3 nanocapsules from nitrate medium *J. Electrochem. Soc.* **158** 12 E136-E41
[37] Wu Y, Chen Y and Zhou J 2013 La (OH) 3 nanorods and La2O3 nanoplates: Facile synthesis and photoluminescence properties *Mater. Lett.* **95** 5-8
[38] Hu C, Liu H, Dong W, Zhang Y, Bao G, Lao C and Wang Z L 2007 La (OH) 3 and La2O3 nanobelts—synthesis and physical properties *Adv. Mater.* **19** 3 470-4
[39] Wang L, Chen J, Ge L, Rudolph V and Zhu Z 2013 Halloysite nanotube supported Ru nanocatalysts synthesized by the inclusion of preformed Ru nanoparticles for preferential oxidation of CO in H2-rich atmosphere *J. Phys. Chem. C* **117** 8 4141-51